

Quantum hardware demonstrations of relativistic calculations of molecular electric dipole moments: from light to heavy systems using Variational Quantum Eigensolver

Palak Chawla,^{1,*} Shweta,^{2,*} K. R. Swain,^{1,†} Tushti Patel,¹ Renu Bala,^{1,‡} Disha Shetty,¹ Kenji Sugisaki,^{1,3,4} Sudhindu Bikash Mandal,¹ Jordi Riu,^{5,6} Jan Nogué,⁵ V. S. Prasanna,^{1,7,§} and B. P. Das^{1,7,8}

¹*Centre for Quantum Engineering, Research and Education, TCG Crest, Kolkata 700091, India*

²*Department of Physics, Indian Institute of Technology Delhi, New Delhi 110016, India*

³*Graduate School of Science and Technology, Keio University,
7-1 Shinkawasaki, Saiwai-ku, Kawasaki, Kanagawa 212-0032, Japan*

⁴*Quantum Computing Center, Keio University, 3-14-1 Hiyoshi,
Kohoku-ku, Yokohama, Kanagawa 223-8522, Japan*

⁵*Qilimanjaro Quantum Tech, Carrer dels Comtes de Bell-Lloc, 161, 08014 Barcelona, Spain*

⁶*Universitat Politècnica de Catalunya, Carrer de Jordi Girona, 3, 08034 Barcelona, Spain*

⁷*Academy of Scientific and Innovative Research (AcSIR), Ghaziabad- 201002, India*

⁸*Department of Physics, Tokyo Institute of Technology,
2-12-1 Ookayama, Meguro-ku, Tokyo 152-8550, Japan*

(Dated: June 10, 2024)

The quantum–classical hybrid Variational Quantum Eigensolver (VQE) algorithm is recognized to be the method of choice to obtain ground state energies of quantum many-body systems in the noisy intermediate scale quantum (NISQ) era. This study not only extends the VQE algorithm to the relativistic regime, but also calculates a property other than energy, namely the molecular permanent electric dipole moment (PDM). We carry out 18-qubit quantum simulations to obtain ground state energies as well as PDMs of single-valence diatomic molecules, ranging from the light BeH to the heavy radioactive RaH molecule. We investigate the correlation trends in these systems as well as access the precision in our results. Furthermore, we measure the PDM of the moderately heavy SrH and SrF molecules on the optimized unitary coupled cluster state, using the state-of-the-art IonQ Aria-I quantum computer in an active space of 6 qubits. The associated quantum circuits for these computations were extensively optimized in view of limitations imposed by NISQ hardware. To that end, we employ an array of techniques, including the use of point group symmetries, integrating ZX-Calculus into our pipeline-based circuit optimization, and energy sort VQE procedure. Through these methods, we compress our 6-qubit quantum circuit from 280 two-qubit gates to 37 two-qubit gates (with a marginal trade-off of 0.33 and 0.31 percent in the PDM for SrH and SrF in their respective 6-spin orbital active spaces). We anticipate that our proof-of-concept demonstration lays the groundwork for future quantum hardware calculations involving heavy atoms and molecules.

I. INTRODUCTION

The electronic structure problem is computationally very challenging, owing to the exponential growth of the state space with system size. However, since the dynamics of electrons in atoms and molecules is governed by quantum mechanics, it can be efficiently simulated on quantum computers via suitable quantum algorithms, thus leading to better scaling over the corresponding state-of-the-

art counterparts on conventional computers [1–3]. The quantum phase estimation algorithm [3–5] was proposed to efficiently solve atomic and molecular problems on a quantum computer. However, given the limitations imposed by noisy intermediate scale quantum era devices and the fact that the depth of the quantum phase estimation quantum circuit grows rapidly with system size, the algorithm is better suited for the fault-tolerant quantum computing era [6]. However, the quantum–classical hybrid variational quantum eigensolver (VQE) algorithm comes with relatively shallow circuits, thus allowing one to apply it to electronic structure problems on currently available quantum computers [7].

Thus far, the VQE algorithm has predominantly been employed to calculate ground state energies and first ionization energies of atomic, molecular and ionic systems [8–14]. It has also been experimentally realized on differ-

* Contributed equally to the work

† Current address: Department of Physics and Materials Science, University of Luxembourg, L-1511 Luxembourg, Luxembourg

‡ Current address: Institute of Physics, Faculty of Physics, Astronomy and Informatics, Nicolaus Copernicus University, Grudziadzka 5, 87-100 Toruń, Poland

§ srinivasaprasanna@gmail.com

ent quantum hardware platforms [15–25]. However, there are not many works that calculate atomic and molecular properties besides energies [10, 26, 27]. Further, to the best of our knowledge, only one work treats relativistic effects in such systems [28] within the framework of the VQE algorithm. There are a few studies that incorporate relativistic effects in the context of other quantum computing algorithms [29–32].

In this work, we calculate the molecular permanent electric dipole moments (PDMs) of single-valence molecular systems, by implementing the VQE algorithm in a relativistic framework. The PDM is an important molecular property. It finds its use in the search for novel quantum phases including the elusive supersolid phase [33], in the study of dipole–dipole molecular interactions with implications in, for example, quantum computing [34], and in fundamental physics searches via the polarization factor [35]. Our choice of molecules spans the single-valence alkaline earth metal monohydrides (including the radioactive and heavy RaH molecule, where relativistic effects become important), all of which carry the potential to be laser cooled [36, 37]. Notably, CaH and BaH have already been laser cooled [38, 39]. Furthermore, we carry out resource-reduced 6-qubit computations (with error mitigation) of the PDMs of SrH and SrF molecules on the IonQ Aria-I quantum hardware, by measuring the PDM operator on the optimized unitary coupled cluster singles and doubles (UCCSD) state. We expect that our work would not only serve as a first step in determining the PDMs of more complex molecules, but also would open new avenues in exploring several other atomic and molecular properties of interest to various applications such as new physics beyond standard model of elementary particles, where the effects of relativity become prominent [40, 41].

We discuss the theory and the methodology adopted in our work, in Section II. This is followed by Section III, where we present the results obtained for the ground state energies and PDMs of the chosen molecules using the VQE algorithm for relativistic regime. We finally conclude in Section IV.

II. THEORY AND METHODOLOGY

A. The VQE algorithm: a primer

Given a many-body Hamiltonian (\hat{H}) and a trial wavefunction, $|\Psi(\theta)\rangle$, where $\{\theta\} \in \{\theta_1, \theta_2, \dots\}$, minimizing an energy functional ($E(\theta)$) with respect to $\{\theta\}$ yields an energy that is an upper bound to the true ground state

value, E_0 . Mathematically, we can express it as

$$E(\theta) = \frac{\langle \Psi(\theta) | \hat{H} | \Psi(\theta) \rangle}{\langle \Psi(\theta) | \Psi(\theta) \rangle} \geq E_0. \quad (1)$$

The above statement conveys the essence of the Rayleigh–Ritz variational principle [42]. $|\Psi(\theta)\rangle$ should be realizable as a parametrized quantum circuit so that it can be executed on a quantum device. In our work, we choose our ansatz, that is, the functional form for $\hat{U}(\theta)$ that occurs in $|\Psi(\theta)\rangle = \hat{U}(\theta) |\Phi_0\rangle$, to be the unitary coupled cluster ansatz [43, 44], which is given as

$$\begin{aligned} |\Psi(\theta)\rangle &= e^{\hat{T} - \hat{T}^\dagger} |\Phi_0\rangle \\ &= e^{\hat{T}} |\Phi_0\rangle, \end{aligned} \quad (2)$$

where $|\Phi_0\rangle$ is the initial/reference Hartree–Fock (HF) state, and $\hat{T} = \hat{T}_1 + \hat{T}_2 + \dots + \hat{T}_N$ for an N -electron system, where $\hat{T}_1 = \sum_{i,a} \theta_i^a \hat{a}_a^\dagger \hat{a}_i$ accounts for all possible one particle–one hole excitations, $\hat{T}_2 = \sum_{i,j,a,b} \theta_{ij}^{ab} \hat{a}_a^\dagger \hat{a}_b^\dagger \hat{a}_j \hat{a}_i$ considers all possible two particle–two hole excitations, etc. \hat{a}_a^\dagger and \hat{a}_i are fermionic creation and annihilation operators, which create and annihilate an electron in spin orbitals a and i , respectively. We have used the subscripts i and j for occupied, a and b for unoccupied, and p, q, r , and s for general spin orbitals throughout this work. Further, we consider only the single (S) and double (D) excitations, and hence the employed UCCSD ansatz is given by $e^{\hat{T}} = e^{\hat{T}_1 + \hat{T}_2}$. The energy functional in Eq. (1) now becomes

$$E(\theta) = \langle \Phi_0 | e^{\hat{T}^\dagger(\theta)} \hat{H} e^{\hat{T}(\theta)} | \Phi_0 \rangle. \quad (3)$$

It is worth mentioning at this point that approaches based on the coupled cluster method have been found to be most suitable for calculations of atomic and molecular properties [45, 46]. In the unitary coupled cluster approach, the usual CC method is modified to be both variational and unitary, and therefore it is amenable for implementation on a quantum computer while retaining the predictive ability of the traditional CC method.

The molecular many-body Hamiltonian, \hat{H} , can be written in the second quantized notation as

$$\hat{H} = \sum_{p,q} h_{pq} \hat{a}_p^\dagger \hat{a}_q + \frac{1}{2} \sum_{p,q,r,s} h_{pqrs} \hat{a}_p^\dagger \hat{a}_q^\dagger \hat{a}_s \hat{a}_r. \quad (4)$$

The summation is over the number of spin orbitals, which depends on the choice of the employed single particle basis set. h_{pq} and h_{pqrs} are the one- and two-electron integrals, respectively.

We utilise the Jordan–Wigner mapping [47] to transform the Hamiltonian described in Eq. (4) to a sum of tensor products of Pauli operators. The transformed Hamiltonian is given by

$$\hat{H}' = \sum_m^M \alpha_m \hat{P}_m, \quad (5)$$

where α_m are real scalar coefficients which depend on h_{pq} and h_{pqrs} . P_m are Pauli strings represented by tensor products of Pauli operators $\{I, X, Y, Z\}$, and M denotes the number of Pauli strings in the Hamiltonian. Thus, the energy functional can be expressed as

$$E(\theta) = \sum_m^M \alpha_m \langle \Phi'_0 | U'^{\dagger}(\theta) \hat{P}_m U'(\theta) | \Phi'_0 \rangle. \quad (6)$$

where $U'(\theta)$ and $|\Phi'_0\rangle$ refer to the Jordan–Wigner-transformed $U(\theta)$ and $|\Phi_0\rangle$, respectively. Each term in Eq. (6) corresponds to the expectation value of a Pauli string \hat{P}_m , which will be evaluated through statistical sampling on a quantum computer, while the summation and energy minimization will be done on a traditional computer. The energy is minimized by updating the parameters in an iterative process using an appropriate optimization algorithm. In this work, we begin with zero initial parameters and employ the SLSQP (Sequential Least Squares Programming) optimizer [48] to obtain the optimal VQE parameters.

B. The VQE algorithm for relativistic calculations

For a relativistic VQE calculation, we begin with the Dirac–Coulomb Hamiltonian (written in the Born–Oppenheimer approximation and in atomic units), \hat{H}_{DC} , given by

$$\hat{H}_{DC} = \sum_k (c\vec{\alpha} \cdot \vec{p}_k + \beta c^2) + \sum_k V_{nuc}(r_k) + \frac{1}{2} \sum_{k \neq l} \frac{1}{r_{kl}}, \quad (7)$$

where $\vec{\alpha} = \begin{pmatrix} 0 & \vec{\sigma} \\ \vec{\sigma} & 0 \end{pmatrix}$, $\beta = \begin{pmatrix} \mathbb{I} & 0 \\ 0 & -\mathbb{I} \end{pmatrix}$, $\vec{\sigma}$ are the Pauli matrices and \mathbb{I} is the (2×2) identity matrix. The summations are over the number of electrons. $V_{nuc}(r_k)$ refers to the electron–nucleus potential. There is no summation over the number of nuclei, as we consider diatomic molecules in this work and set one of the nuclei

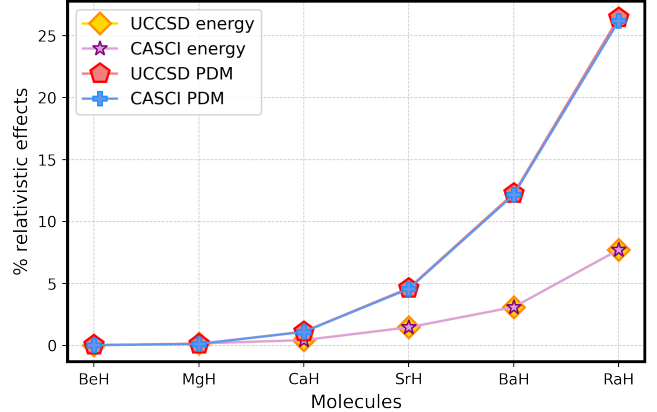


Figure 1. Figure illustrating the % relativistic effects = $\frac{A_{Rel} - A_{NR}}{A_{Rel}} \times 100$ across the alkaline earth metal monohydride systems considered in this work. A can refer to the ground state energy or the PDM. The 18-qubit VQE simulation results for ground state energies and PDMs are benchmarked with results obtained from CASCI calculations.

as the origin. We use finite-sized nuclei (Gaussian) for our relativistic calculations. When the Hamiltonian is converted to its second quantized form, h_{pq} and h_{pqrs} in Eq. (4) are obtained using a suitable relativistic code. Further, $|\Phi_0\rangle$ from Eq. (2) is now the Dirac–Hartree–Fock (DF) state. It is important to stress that since the wavefunction is a four-component spinor, there are more non-zero integrals relative to a non-relativistic computation. For an 18-qubit calculation with 3 occupied and 15 unoccupied spin orbitals, we find that the number of Hamiltonian integrals (the number of Pauli strings, M , in transformed Hamiltonian in Eq. (5)), for example, for RaH are 4, 249 (2, 740) and 47, 099 (12, 556) for the non-relativistic (denoted hereafter as NR for brevity) and relativistic (rel) calculations respectively. Thus, a rel VQE calculation is more resource intensive than its NR counterpart in that the former involves substantially more quantum circuit evaluations per iteration.

For all of our calculations, we choose the following equilibrium bond lengths (in Å): BeH : 1.342 [49], MgH : 1.7297 [49], CaH : 2.0025 [49], SrH : 2.1461 [49], BaH : 2.2319 [49], and RaH : 2.43 [50]. The one- and two-electron (Hamiltonian) integrals as well as the property (PDM) integrals are generated by the DIRAC22 [51] program. This is followed by a VQE-UCCSD computation with Qiskit’s statevector backend [52] to obtain the ground state energy and the wavefunction. The DIRAC22 and the Qiskit programs are interfaced by suitably modi-

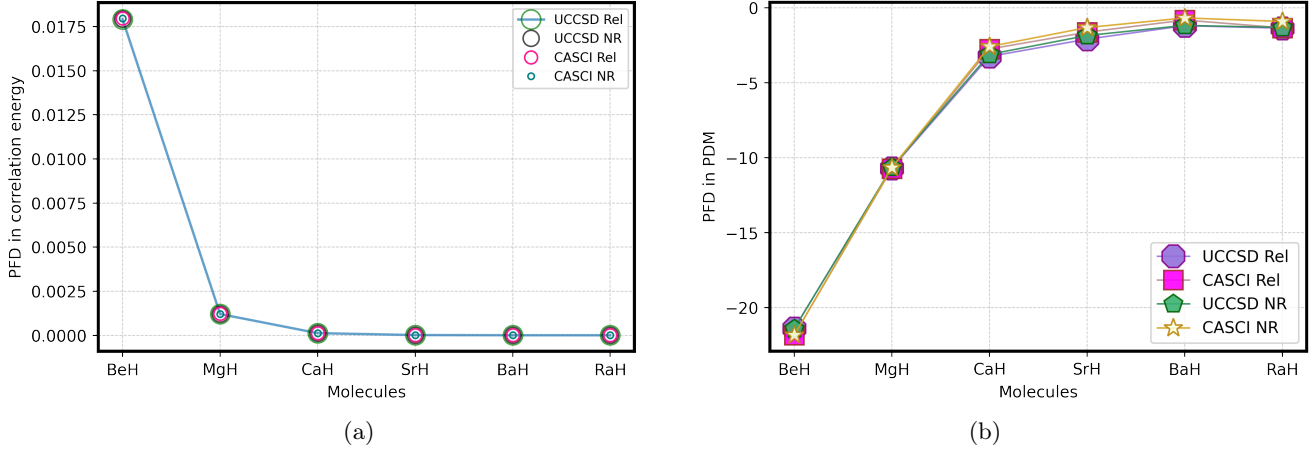


Figure 2. Plots showing (a) the PFD in correlation energy with respect to the total energy at the VQE and CASCI levels of theory, and (b) the PFD in correlation contribution to the PDM with respect to the total PDM using the VQE and CASCI methods.

fyng the OpenFermion–Dirac [51] libraries. We note that for all of the simulations carried out in this work, we employ the uncontracted dyall.v4z basis sets [53], while for the quantum hardware computations, we use the contracted STO-6G basis [54].

Once the wavefunction is known, the PDM is calculated as an expectation value given by $\langle \hat{D} \rangle = \langle \Psi(\theta^*) | \hat{D} | \Psi(\theta^*) \rangle$ for our simulations; where $|\Psi(\theta^*)\rangle$ is the ground state wavefunction constructed from the converged amplitudes (denoted by the superscript, ‘*’) of the VQE algorithm. The dipole moment operator, \hat{D} , contains two terms, nuclear and electronic. The nuclear part contains only one term, since we have chosen one of the two atoms in the diatomic molecule to be positioned at the origin. Therefore, within the Born–Oppenheimer approximation, $\hat{D} = Z_N R_N - \sum_k r_k$, where r_k is the position coordinate of the k^{th} electron from the origin, R_N is the equilibrium bond length of the molecule, and Z_N is the nuclear charge of the second atom which is not at the origin. For the quantum hardware computations, we measure the PDM operator on the converged ground state, $|\Psi(\theta^*)\rangle$. We have benchmarked our VQE–UCCSD PDM values (for 18-qubit simulations as well as 6-qubit hardware executions) with those obtained via complete active space configuration interaction (CASCI) calculations, where we carry out a full CI calculation within a specified active space.

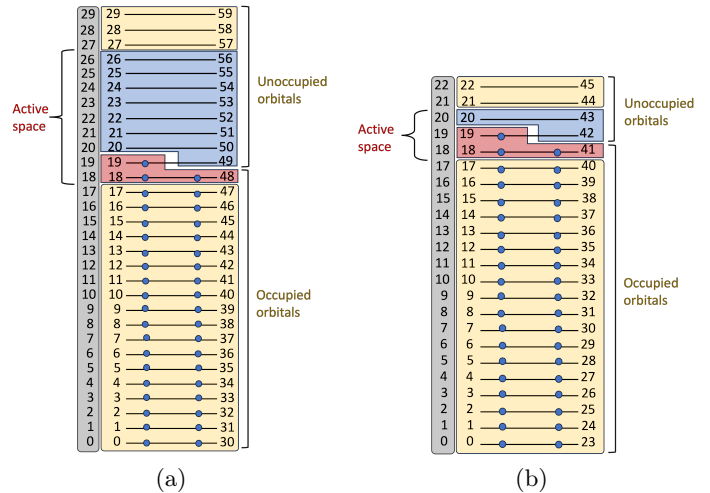


Figure 3. Figure indicating our choice of active space for (a) simulation (18 qubits), and (b) quantum hardware (6 qubits), for the SrH molecule. The same active space size (3 electrons and 6 spin orbitals) is chosen for the SrF 6 qubit–quantum hardware calculation as well. The molecular orbital indices are marked in gray. Orbitals shown in yellow are the ones that are frozen for the relevant calculations.

III. RESULTS AND DISCUSSION

This section is organized as follows: the precision to which our 18-qubit VQE–UCCSD simulations capture relativistic and correlation effects in the ground state energies and PDMs (relative to CASCI) of the systems con-

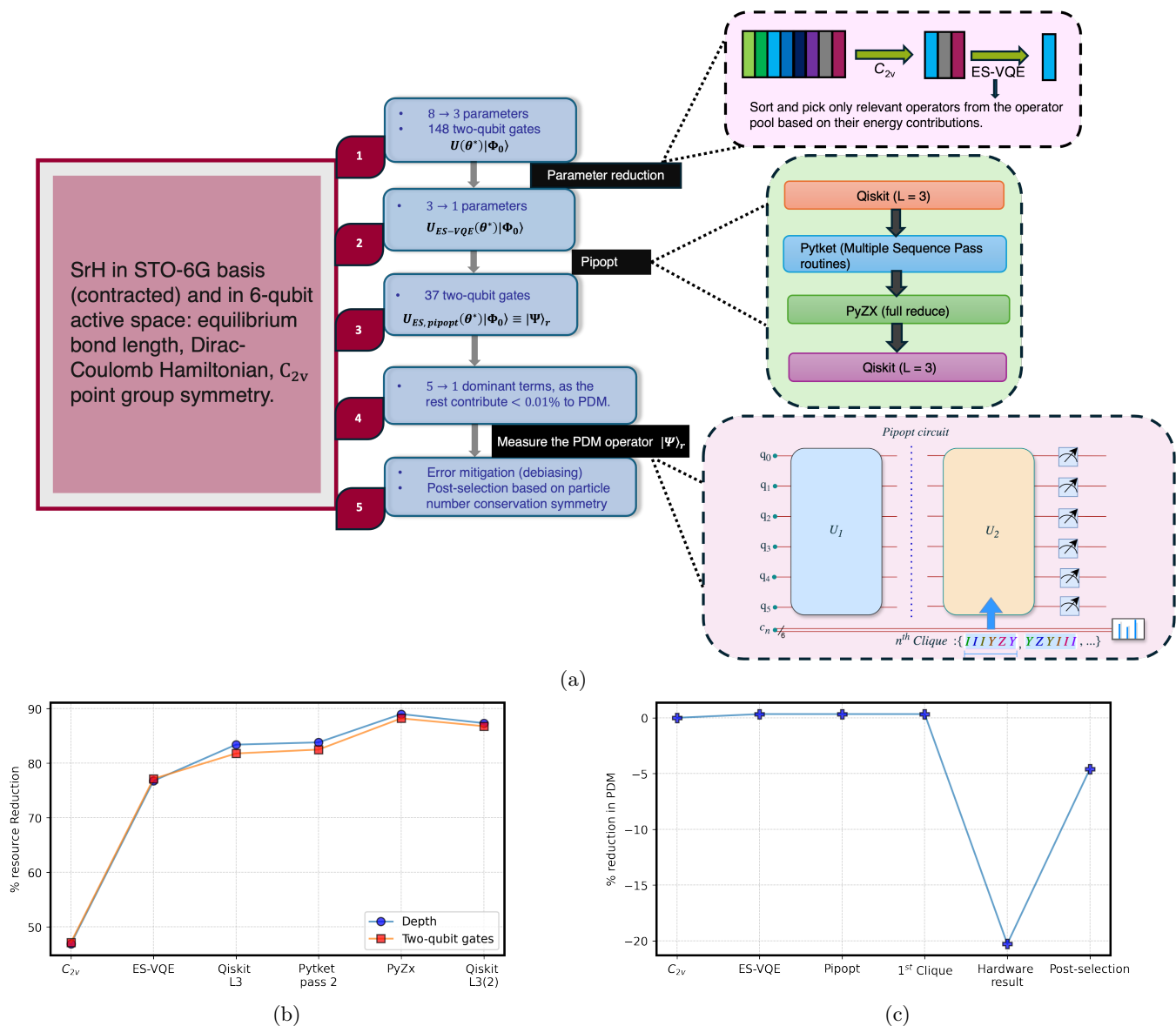


Figure 4. (a) Our workflow for quantum hardware execution on the IonQ Aria-1 device. Our scheme systematically reduces the resources required, as subfigure (b) indicates, while retaining a reasonable precision in predicting the PDM (as subfigure (c) shows). In the figure, U_{ES-VQE} refers to the UCCSD circuit after ES-VQE, whereas $U_{ES, Pipopt}$ is the ES-VQE state after pipeline-based quantum circuit optimization routine. Throughout the figure, we abbreviate pipeline-based quantum circuit optimization as Pipopt. The ‘(2)’ in the last entry on the X-axis of sub-figure (b) refers to the fact that we execute the Qiskit L3 routine for the second time. Further, in sub-figure (c), ‘1st Clique’ refers to the fact that the dominant clique is the very first one (See Table S2 of the Supplemental Material).

sidered in this work are discussed in sub-sections III A and III B respectively. We then comment briefly on the interplay between relativistic and correlation effects, in sub-section III C. Finally, in sub-section III D, we present

details of our 6-qubit quantum hardware computations of the PDMs of the SrH and SrF molecules on the IonQ Aria-I device.

A. Relativistic effects

Figure 1 presents our results for the size of relativistic effects, quantified by % relativistic effects = $\frac{A_{Rel} - A_{NR}}{A_{Rel}} \times 100$, where A can be either the ground state energy or the PDM. Table S1 of the Supplemental Material provides the data for the values of ground state energies and PDMs. It can be seen from the figure that relativistic effects start becoming progressively important as we move from BeH through RaH. In the heaviest RaH molecule that we have considered, relativity accounts for 7.73 percent and 26.47 percent respectively for ground state energy and PDM, indicating that the latter is very sensitive to relativistic effects relative to the former. The figure also demonstrates the ability of the VQE-UCCSD algorithm to capture relativistic effects by comparing the results obtained using the algorithm with those from CASCI values. We add that for the CASCI calculations, we diagonalize the Jordan–Wigner-transformed qubit Hamiltonian by specifying the correct particle number. The CASCI calculations were performed using the OpenFermion package [55]. The disagreement between our VQE-UCCSD and CASCI results are at most 0.47 percent for the CaH molecule. We note that for the case of BaH (NR calculation), the HF calculation using default computational conditions of DIRAC22 converged to the metastable spin-doublet state. To obtain the lowest spin-doublet HF state, we replaced the initial guess orbitals with the HF canonical orbitals obtained for the neighbouring geometry. It is also worth mentioning at this point that our PDM results for BeH and MgH are in reasonable agreement with those obtained from high accuracy calculations [49] (a percentage fraction difference of 2.05 and 3.79 for BeH and MgH respectively). This fortuitous result could be attributed at least in part to the size of the active space in relation to that of these two systems as well as the quality of our basis sets.

B. Correlation effects

We now turn our attention to the role of correlation effects to the ground state energies and PDMs of the considered molecules. Figure 2 presents the percentage fraction difference (PFD), defined as $\frac{A_X - A_{MF}}{A_X} \times 100$, for both ground state energies and PDMs of the considered systems in sub-figures 2(a) and 2(b) respectively. A can either be the ground state energy or the PDM, and X can be VQE-UCCSD or CASCI. MF is HF for non-relativistic cases and DF in a relativistic calculation.

We see from Figure 2(a), which shows the PFDs for ground state energies, that the VQE-UCCSD and the CASCI results agree remarkably well in the amount of cor-

relation energy predicted, to within 0.0175 percent. Figure 2(b) illustrates a similar trend, where VQE-UCCSD and CASCI values agree in their prediction of the correlation contribution to the PDM of the molecules.

C. Interplay of relativistic and correlation effects

To understand the interplay between relativistic and correlation effects, we pick the RaH molecule. We make this choice in view of Figure 1, where our VQE-UCCSD simulation results indicated that, as expected, relativistic effects play a major role in determining the PDM of the heavy RaH molecule. The effect of correlation is to decrease the PDM, and it does so by 1.32 and 1.36 percent for NR and rel cases respectively. On the other hand, we find that the effect of relativity is to increase the PDM by 26.50 and 26.47 percent at the mean field and correlated levels of theory, respectively. The net effect of relativity and correlation changes the PDM from 1.1306 atomic units to 1.5177 atomic units, a change of 25.51 percent.

D. Quantum hardware computations

In this subsection, we present our proof-of-principle quantum hardware results of PDMs in the relativistic VQE framework. We intend that our computations on quantum hardware not only serve as a proof-of-principle demonstration of relativistic VQE applied to property computations, but also reflect the current capabilities of quantum hardware. To that end, we compute PDMs in an active space of 6 qubits on the SrH molecule in the STO-6G basis using one of the best commercial quantum computers available currently, the IonQ Aria-I device. Figure 3 shows the active space choices for the SrH molecule for our 18-qubit simulation and 6-qubit hardware computation. We choose the SrH molecule as a representative candidate to demonstrate our quantum hardware results, as the molecule is moderately heavy, just enough to display relativistic effects in its PDM. Before executing our resource-reduced hardware demonstrations, we benchmark our simulated VQE-UCCSD PDM values with their corresponding CASCI counterparts to ensure that the former results are in good agreement with the best possible ones for our considered 6-qubit active space. We find that our results are in good agreement with the CASCI ones, with PFDs of 0.24 and 0.26 for SrH and SrF respectively. Our workflow, illustrated in Figure 4(a), involves measuring the PDM of a molecule on a doubly optimized UCCSD state, where not only are the parameters

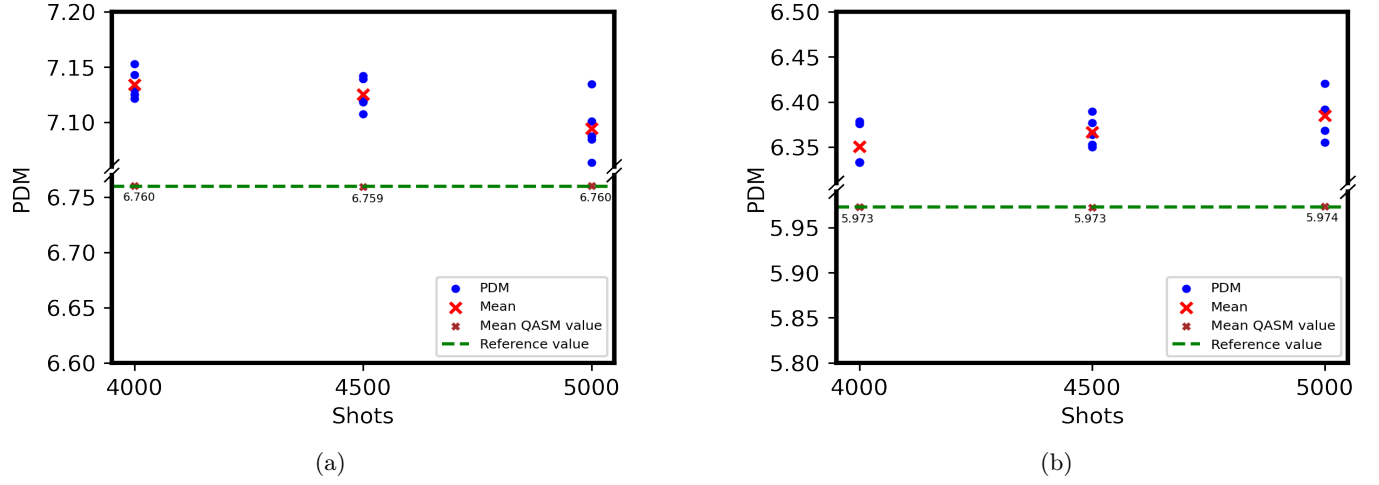


Figure 5. Our results for the PDM (in atomic units) of (a) SrH and (b) SrF molecules in an active space of 6 qubits with varying number of shots and five repeats per shot number, obtained on the 25-qubit universal gate-model ion-trap quantum hardware, Aria-1, after error mitigation and post-selection strategies. For our main results, we consider the data obtained using 5000 shots.

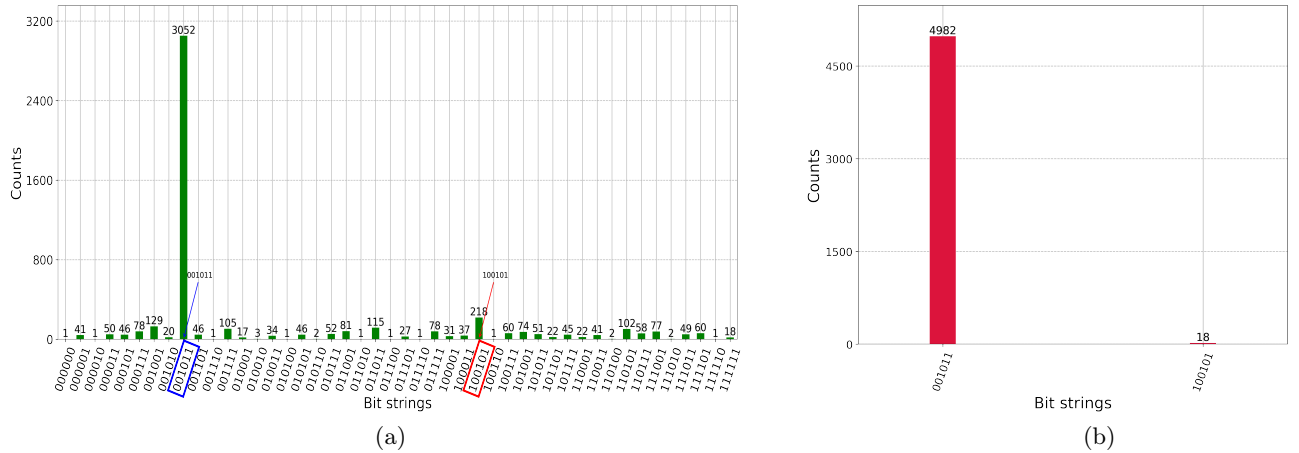


Figure 6. Sub-figures presenting the results after measuring the PDM on (a) the Aria-I quantum device and (b) on the Qiskit QASM backend.

optimized via a VQE procedure carried out on a traditional computer, but also the resulting circuit is obtained via multiple resource reduction steps. Our workflow involves the following steps:

1. We leverage the C_{2v} point group symmetry to reduce gate count (via reducing parameter count), using the procedure prescribed in Ref. [56]. This implementation leads to a substantial reduction in number of parameters, from 8 to 3, for SrH. In our quantum circuit, this has the effect of lowering the number of two-qubit gates from 280 to 148.
2. We then carry out a VQE procedure to obtain the optimized UCCSD parameters. We denote such a state as $U(\theta^*)|\Phi_0\rangle$.
3. We perform an energy sort VQE (ES-VQE) procedure [57] to pick the most important excitation (two electron excitation operator to generate $|100101\rangle$ from $|001011\rangle$). The resulting circuit has 64 two-qubit gates. It is important to note that the percentage loss in the value of PDM for SrH is only 0.33.

4. We then pass the quantum circuit through a sequence of circuit optimization routines. We call this the pipeline-based optimization process, and it is based on the approach taken in Ref. [58]. In our case, since the circuit is dominated by Cliffords, we also use the ZX-Calculus based routine, PyZX [59]. Our pipeline involves: Qiskit L3 [52]–Pytket (multiple sequence pass routines) [60]–PyZX (full reduce)–Qiskit (L3). We tried several combinations of optimization routines, and found that this specific choice gives the best results in terms of reducing circuit depth while retaining accuracy. We then transpile the circuit into a verbatim one (that is, in the native gate set of the target quantum device). At the end of this procedure, we have 37 two-qubit gates. The step-by-step reduction in resources, that is, the number of two-qubit gates and depth, is shown in Figure 4(b). Throughout this process, we take special care to ensure that a resultant circuit at each step produces a PDM consistent with that of the pre-pipeline quantum circuit.
5. The qubit operator form of the PDM operator contains 19 terms. However, not all of the terms need to be measured on $U(\theta^*)|\Phi_0\rangle$, if one groups the terms into qubit-wise commuting cliques. Further, we choose only the most dominant clique for our quantum hardware computation (for details, see Table S2 of the Supplemental Material). We achieve a tremendous reduction in resources with no loss in PDM, since we find that the first clique is the only one with non-zero contribution to total PDM for the 1-parameter $|\Psi(\theta^*)\rangle$ obtained after ES-VQE.
6. After executing the calculation on a quantum device along with the in-built debiasing mitigation technique [61], we post-select the particle number-conserving bit strings [62, 63], followed by obtaining the PDM. The results from our resource reduction scheme is presented in Figure 4(c).

We now discuss the results obtained using our workflow, from our quantum hardware computations on the Aria-I (6-qubit calculations) device. Although the main system of interest to us is the SrH molecule, we also carried out 6-qubit computations on the comparably heavy and laser-coolable SrF molecule [64–66]. Figures 5(a) and 5(b) present our results for the PDMs of the SrH and SrF molecules, respectively. The plots show that our hardware results, averaged over five repetitions for a given number of shots, upon error mitigation and post-selection, predicts PDMs whose PFD with respect to the statevector

results (for 1-parameter $|\Psi(\theta^*)\rangle_r$) for the same active space is about 4.94 percent for SrH and about 6.90 percent for SrF. Note that, we do not add nuclear and HF core contribution values to the PDM. We note that the two-qubit gate fidelity for the Aria-I device during our computations was about 98.43 percent.

Sub-figure (a) of Figure 6 presents the statistics obtained after measuring the PDM operator on the IonQ Aria-I device, whereas sub-figure (b) presents the same data but on the noiseless QASM backend from Qiskit. The bit strings are specified in the block spin notation, that is, if we read from right to left all the alpha spin orbitals are specified first, followed by the beta spin orbitals, both in the occupancy number representation. The dominant ‘001011’ bit string specifies the HF state, and the next dominant one, that is, ‘100101’, specifies a double excitation that contributes the most to the correlation part of the PDM relative to others. The figures show that we are able to effectively capture both of these bit strings on hardware.

We now briefly comment on existing VQE works that employed the unitary coupled cluster ansatz to carry out molecular calculations on real quantum hardware. Surveys that are more diverse in their range of ansatz and applications can be found in Refs. [67, 68]. Typically, the works involve resource reduction strategies that aim to reduce the number of qubits and/or number of gates and/or the number of VQE iterations in combination with error mitigation techniques to predict ground state energies or potential energy curves of molecular systems [69–75]. However, it is worth noting that some of the works extend the scope of VQE to compute properties such as excitation energies of molecules (for example, see the work on equation of motion VQE described in Ref. [76]). In our work, we implement a relativistic version of the VQE algorithm to compute PDMs of light to heavy molecules. We employ a suite of resource reduction strategies as mentioned in the previous paragraphs of this sub-section, and include error mitigation and post-selection strategies to obtain fairly precise estimates of the PDMs of our target molecules.

IV. CONCLUSION

We have implemented and employed the relativistic version of the VQE algorithm and applied it to the calculation of ground state energies as well as molecular PDMs of a range of single-valence polar diatomic molecules, beginning from the lightest BeH to the heaviest RaH of the alkaline earth metal monohydride series. We benchmark the results of our 18-qubit simulations with the

CASCI approach, both in the non-relativistic and relativistic frameworks. We elucidate the role of correlation as well as relativistic effects, and their interplay in determining the final results. We find from our VQE simulations that the precision with which the algorithm captures relativistic effects in the PDM is at least 99.72 percent (for the case of RaH). Furthermore, we carry out 6-qubit quantum hardware computations of the PDM of SrH as well as that of the SrF molecule on the IonQ Aria-I device. We implement a suite of resource reduction strategies, including leveraging point group symmetry, using energy sort VQE, pipeline-based quantum circuit optimization, qubit-wise commuting cliques, and finally post-selection on the basis of particle number conserving symmetry, and obtain PDMs of SrH and SrF with about 95.06 and 93.10 percent precision relative to the pipeline optimized ES-VQE-UCCSD simulation values obtained on the statevector backend. We anticipate that with further advancements in quantum hardware, the relativistic VQE algorithm will be able to handle heavier molecular systems in larger active spaces and open new avenues for novel applications such as probing new physics beyond the Standard Model of elementary particles.

ACKNOWLEDGMENTS

All our calculations were carried out on the Rudra cluster from SankhyaSutra Labs, Bangalore and on the Airawat HPC cluster, CDAC Pune. KS acknowledges support from Quantum Leap Flagship Program (Grant No. JPMXS0120319794) from the MEXT, Japan, Center of Innovations for Sustainable Quantum AI (JP-MJPF2221) from JST, Japan, and Grants-in-Aid for Scientific Research C (21K03407) and for Transformative Research Area B (23H03819). BPD, VSP, and others acknowledge support from MeitY-AWS Braket QCAL project (N-21/17/2020-NeGD, 2022-24). We would like to acknowledge Dr. V. P. Majety (Indian Institute of Technology Tirupati) for useful discussions with him. Shweta acknowledges Dr. Bodhaditya Santra and members of CAQT lab (Indian Institute of Technology Delhi) for their support during completion of this project. VSP acknowledges support from Mr. Nishanth Baskaran, Dr. Anjani Priya, as well as Dr. Jean-Christophe and Dr. Daniela for support in different aspects of the AWS Braket execution of our workflow. PC acknowledges Mr. Peniel B. Tsemo for useful discussions.

-
- [1] Z. Huang and S. Kais, *Chemical Physics Letters* **413**, 1 (2005).
- [2] R. Xia, Purdue University Graduate School PhD thesis (2020).
- [3] D. S. Abrams and S. Lloyd, *Physical Review Letters* **83**, 5162 (1999).
- [4] A. Y. Kitaev, arXiv preprint quant-ph/9511026 (1995).
- [5] A. Aspuru-Guzik, A. D. Dutoi, P. J. Love, and M. Head-Gordon, *Science* **309**, 1704 (2005).
- [6] D. Bluvstein *et al.*, *Nature* **626**, 58 (2024).
- [7] A. Peruzzo, J. McClean, P. Shadbolt, M.-H. Yung, X.-Q. Zhou, P. J. Love, A. Aspuru-Guzik, and J. L. O’Brien, *Nature Communications* **5**, 4213 (2014).
- [8] M. Ostaszewski, E. Grant, and M. Benedetti, *Quantum* **5**, 391 (2021).
- [9] H. L. Tang, V. Shkolnikov, G. S. Barron, H. R. Grimsley, N. J. Mayhall, E. Barnes, and S. E. Economou, *PRX Quantum* **2**, 020310 (2021).
- [10] R. Villela, V. S. Prasanna, and B. P. Das, *The European Physical Journal Plus* **137**, 1017 (2022).
- [11] Sumeet, S. Prasanna V, B. P. Das, and B. K. Sahoo, *Quantum Reports* **4**, 173 (2022).
- [12] K. Bharti *et al.*, *Reviews of Modern Physics* **94**, 015004 (2022).
- [13] J. Tilly *et al.*, *Physics Reports* **986**, 1 (2022).
- [14] M. Motta and J. E. Rice, *WIREs Computational Molecular Science* **12** (2021).
- [15] A. Kandala, A. Mezzacapo, K. Temme, M. Takita, M. Brink, J. M. Chow, and J. M. Gambetta, *Nature* **549**, 242 (2017).
- [16] P. J. J. O’Malley *et al.*, *Physical Review X* **6**, 031007 (2016).
- [17] Y. Nam *et al.*, *npj Quantum Information* **6**, 33 (2020).
- [18] J. E. Rice, T. P. Gujarati, M. Motta, T. Y. Takeshita, E. Lee, J. A. Latone, and J. M. Garcia, *The Journal of Chemical Physics* **154**, 134115 (2021).
- [19] Q. Gao, H. Nakamura, T. P. Gujarati, G. O. Jones, J. E. Rice, S. P. Wood, M. Pistoia, J. M. Garcia, and N. Yamamoto, *The Journal of Physical Chemistry A* **125**, 1827 (2021).
- [20] M. Motta, G. O. Jones, J. E. Rice, T. P. Gujarati, R. Sakuma, I. Liepuoniute, J. M. Garcia, and Y.-y. Ohnishi, *Chemical Science* **14**, 2915 (2023).
- [21] C. Hempel *et al.*, *Physical Review X* **8**, 031022 (2018).
- [22] S. E. Smart and D. A. Mazziotti, *Physical Review A* **100**, 022517 (2019).
- [23] F. Arute *et al.*, *Science* **369**, 1084 (2020).
- [24] A. J. McCaskey, Z. P. Parks, J. Jakowski, S. V. Moore, T. D. Morris, T. S. Humble, and R. C. Pooser, *npj Quantum Information* **5**, 99 (2019).
- [25] Y. Shen, X. Zhang, S. Zhang, J.-N. Zhang, M.-H. Yung, and K. Kim, *Physical Review A* **95**, 020501 (2017).
- [26] S. T. Stober, S. M. Harwood, D. Trennev, P. K. Barkoutsos, T. P. Gujarati, and S. Mostame, *Physical Review A*

- 105**, 012425 (2022).
- [27] R. M. Parrish, E. G. Hohenstein, P. L. McMahon, and T. J. Martínez, *Physical Review Letters* **122**, 230401 (2019).
- [28] V. Zaytsev, M. Groshev, I. Maltsev, A. Durova, and V. Shabaev, *International Journal of Quantum Chemistry* **124**, e27232 (2024).
- [29] L. Veis, J. Višňák, T. Fleig, S. Knecht, T. Saue, L. Visscher, and J. Pittner, *Physical Review A* **85**, 030304 (2012).
- [30] T. F. Stetina, A. Ciavarella, X. Li, and N. Wiebe, *Quantum* **6**, 622 (2022).
- [31] K. Sugisaki, V. Prasanna, S. Ohshima, T. Katagiri, Y. Mochizuki, B. Sahoo, and B. Das, *Electronic Structure* **5**, 035006 (2023).
- [32] V. Kumar, N. Baskaran, V. S. Prasanna, K. Sugisaki, D. Mukherjee, K. G. Dyllal, and B. P. Das, *Physical Review A* **109**, 042808 (2024).
- [33] T. Mishra, R. V. Pai, S. Ramanan, M. S. Luthra, and B. P. Das, *Physical Review A* **80**, 043614 (2009).
- [34] D. DeMille, *Physical Review Letters* **88**, 067901 (2002).
- [35] A. C. Vutha *et al.*, *Journal of Physics B: Atomic, Molecular and Optical Physics* **43**, 074007 (2010).
- [36] Y. Gao and T. Gao, *Physical Review A* **90**, 052506 (2014).
- [37] R. Pang *et al.*, *ACS Omega* **8**, 19391 (2023).
- [38] R. L. McNally, I. Kozryev, S. Vazquez-Carson, K. Wenz, T. Wang, and T. Zelevinsky, *New Journal of Physics* **22**, 083047 (2020).
- [39] S. Vázquez-Carson, Q. Sun, J. Dai, D. Mitra, and T. Zelevinsky, *New Journal of Physics* **24**, 083006 (2022).
- [40] V. S. Prasanna, A. C. Vutha, M. Abe, and B. P. Das, *Physical Review Letters* **114**, 183001 (2015).
- [41] D. DeMille, S. B. Cahn, D. Murphree, D. A. Rahmlow, and M. G. Kozlov, *Physical Review Letters* **100**, 023003 (2008).
- [42] S. H. Gould, *Variational Methods for Eigenvalue Problems* (University of Toronto Press, 1966).
- [43] A. G. Taube and R. J. Bartlett, *International Journal of Quantum Chemistry* **106**, 3393 (2006).
- [44] A. Anand *et al.*, *Chemical Society Reviews* **51**, 1659 (2022).
- [45] M. Abe, G. Gopakumar, M. Hada, B. P. Das, H. Tatewaki, and D. Mukherjee, *Physical Review A* **90**, 022501 (2014).
- [46] V. S. Prasanna, A. C. Vutha, M. Abe, and B. P. Das, *Physical Review Letters* **114**, 183001 (2015).
- [47] P. Jordan and E. Wigner, *Zeitschrift für Physik* **47**, 631 (1928).
- [48] D. Kraft, *A Software Package for Sequential Quadratic Programming* (Wiss. Berichtswesen d. DFVLR, 1988).
- [49] N. M. Fazil, V. S. Prasanna, K. V. P. Latha, M. Abe, and B. P. Das, *Physical Review A* **98**, 032511 (2018).
- [50] N. M. Fazil, V. S. Prasanna, K. V. P. Latha, M. Abe, and B. P. Das, *Physical Review A* **99**, 052502 (2019).
- [51] DIRAC, a relativistic ab initio electronic structure program, Release DIRAC22 (2022), written by H. J. Aa. Jensen *et al.* (available at [http://www.diracprogram.org](http://dx.doi.org/10.5281/zenodo.6010450)).
- [52] M. Treinish *et al.*, Qiskit: An open-source framework for quantum computing (2022).
- [53] K. G. Dyllal, *The Journal of Physical Chemistry A* **113**, 12638 (2009).
- [54] B. P. Pritchard, D. Altarawy, B. Didier, T. D. Gibson, and T. L. Windus, *Journal of Chemical Information and Modeling* **59**, 4814 (2019).
- [55] J. R. McClean *et al.*, *Quantum Science and Technology* **5**, 034014 (2020).
- [56] C. Cao *et al.*, *Physical Review A* **105**, 062452 (2022).
- [57] Y. Fan, C. Cao, X. Xu, Z. Li, D. Lv, and M.-H. Yung, *The Journal of Physical Chemistry Letters* **14**, 9596 (2023).
- [58] Y. Kharkov, A. Ivanova, E. Mikhantiev, and A. Kotelnikov, arXiv preprint arXiv:2202.14025 (2022).
- [59] A. Kissinger and J. van de Wetering, in *Proceedings 16th International Conference on Quantum Physics and Logic*, Chapman University, Orange, CA, USA., 10-14 June 2019, *Electronic Proceedings in Theoretical Computer Science*, Vol. 318, edited by B. Coecke and M. Leifer (Open Publishing Association, 2020) pp. 229–241.
- [60] S. Sivarajah, S. Dilkes, A. Cowtan, W. Simmons, A. Edgington, and R. Duncan, *Quantum Science and Technology* **6**, 014003 (2020).
- [61] A. Maksymov, J. Nguyen, Y. Nam, and I. Markov, Enhancing quantum computer performance via symmetrization (2023), arXiv:2301.07233 [quant-ph].
- [62] X. Bonet-Monroig, R. Sagastizabal, M. Singh, and T. E. O’Brien, *Physical Review A* **98**, 062339 (2018).
- [63] J. Goings, L. Zhao, J. Jakowski, T. Morris, and R. Pooser, in *2023 IEEE International Conference on Quantum Computing and Engineering (QCE)* (IEEE Computer Society, Los Alamitos, CA, USA, 2023) pp. 76–82.
- [64] E. S. Shuman, J. F. Barry, and D. DeMille, *Nature* **467**, 820 (2010).
- [65] E. B. Norrgard, D. J. McCarron, M. H. Steinecker, M. R. Tarbutt, and D. DeMille, *Physical Review Letters* **116**, 063004 (2016).
- [66] M. Steinecker, D. McCarron, Y. Zhu, and D. DeMille, *ChemPhysChem* **17**, 3664 (2016).
- [67] T. Angelides, P. Naredi, A. Crippa, K. Jansen, S. Kühn, I. Tavernelli, and D. S. Wang, (2024), arXiv:2312.12831 [hep-lat].
- [68] K. Lively, T. Bode, J. Szangolies, J.-X. Zhu, and B. Fauseweh, arXiv preprint arXiv:2402.18953 (2024).
- [69] S. Guo, J. Sun, H. Qian, M. Gong, Y. Zhang, F. Chen, Y. Ye, Y. Wu, S. Cao, K. Liu, *et al.*, arXiv preprint arXiv:2212.08006 (2022).
- [70] H. Shang, X. Zeng, M. Gong, Y. Wu, S. Guo, H. Qian, C. Zha, Z. Fan, K. Yan, X. Zhu, *et al.*, arXiv preprint arXiv:2405.09164 (2024).
- [71] S. Sun, C. Kumar, K. Shen, E. Shishenina, and C. B. Mendl, Evaluating ground state energies of chemical systems with low-depth quantum circuits and high accuracy (2024), arXiv:2402.13960 [quant-ph].

- [72] G. R. Dahale, in *2023 IEEE International Conference on Quantum Computing and Engineering (QCE)*, Vol. 2 (IEEE, 2023) pp. 89–93.
- [73] L. Zhao, J. J. Goings, K. Shin, W. Kyoung, J. I. Fuks, J.-K. K. Rhee, Y. M. Rhee, K. Wright, J. H. V. Nguyen, J. Kim, and S. Johri, *npj Quantum Information* **9**, 1 (2022).
- [74] C. Sarma, O. Di Matteo, A. Abhishek, and P. C. Srivastava, *Physical Review C* **108**, 064305 (2023).
- [75] L. Zhao, J. Goings, Q. Wang, K. Shin, W. Kyoung, S. Noh, Y. M. Rhee, and K. Kim, arXiv preprint arXiv:2312.05426 (2023).
- [76] P. J. Ollitrault *et al.*, *Physical Review Research* **2**, 043140 (2020).

Table S1. Table presenting the ground state energies and PDMs (includes frozen core and nuclear contributions along with the active space contribution) of the considered molecules from different methods. The list of abbreviations used are HF: Hartree-Fock, DF: Dirac-Fock, VQE: VQE with UCCSD ansatz, NR: non-relativistic, Rel: relativistic, CASCI: Complete Active Space Configuration Interaction. Our main results for this work are marked in bold font. The energy is in units of Hartree, whereas the PDM is given in atomic units.

Molecule	Method	Energy	PDM
BeH	HF	-15.153224	0.1137
	DF	-15.156052	0.1137
	VQE (NR)	-15.155941	0.0936
	VQE (Rel)	-15.158768	0.0937
	CASCI (NR)	-15.155949	0.0933
	CASCI (Rel)	-15.158776	0.0933
MgH	HF	-200.157231	0.5850
	DF	-200.477277	0.5861
	VQE (NR)	-200.159639	0.5288
	VQE (Rel)	-200.479695	0.5295
	CASCI (NR)	-200.159665	0.5287
	CASCI (Rel)	-200.479722	0.5294
CaH	HF	-677.314268	0.8269
	DF	-680.265163	0.8374
	VQE (NR)	-677.315076	0.8020
	VQE (Rel)	-680.265994	0.8111
	CASCI (NR)	-677.315085	0.8061
	CASCI (Rel)	-680.266003	0.8150
SrH	HF	-3132.103015	0.9829
	DF	-3178.633202	1.0331
	VQE (NR)	-3132.103414	0.9650
	VQE (Rel)	-3178.633645	1.0119
	CASCI (NR)	-3132.103417	0.9701
	CASCI (Rel)	-3178.633649	1.0165
BaH	HF	-7884.116035	0.9510
	DF	-8136.206375	1.0843
	VQE (NR)	-7884.116240	0.9400
	VQE (Rel)	-8136.206603	1.0715
	CASCI (NR)	-7884.116240	0.9446
	CASCI (Rel)	-8136.206609	1.0755
RaH	HF	-23094.88059	1.1306
	DF	-25028.73616	1.5383
	VQE (NR)	-23094.88079	1.1159
	VQE (Rel)	-25028.73645	1.5177
	CASCI (NR)	-23094.8808	1.1203
	CASCI (Rel)	-25028.7365	1.5180

Table S2. Table presenting the clique-wise contribution to PDM at HF and correlated levels for SrH and SrF in an active space of six spin orbitals with 1-parameter VQE statevector calculation. For this case, the entire contribution to the PDM, both at mean field level and correlated level, comes from Pauli strings containing only I and Z . For a given molecule, each row is a clique (qubit-wise commuting), and lists the number of Pauli words in each clique.

Molecule	Terms	$\langle \Phi_0 \hat{D} \Phi_0 \rangle$	$\langle \Psi_r \hat{D} \Psi_r \rangle$	Correlation in PDM (a.u.)
SrH	IIIII , IIIHZ, IIIZI, IIIZI, IIZII, IIZII, IZIII, ZIIII	6.75406	6.75997	0.00591
	IIIIY, IIIYI, IYYIII, YYIII	0	0	0
	IIIIX, IIIXI, IXXIII, XXIII	0	0	0
	IIYZY, YZYIII	0	0	0
	IIIXZ, XZXIII	0	0	0
SrF	IIIII , IIIHZ, IIIZI, IIIZI, IIZII, IIZII, IZIII, ZIIII	5.96841	5.97296	0.00455
	IIIIY, IIIYI, IYYIII, YYIII	0	0	0
	IIIIX, IIIXI, IXXIII, XXIII	0	0	0
	IIYZY, YZYIII	0	0	0
	IIIXZ, XZXIII	0	0	0